

IMPACTS OF NICER'S RADIUS MEASUREMENT OF PSR J0740+6620 ON NUCLEAR SYMMETRY ENERGY AT SUPRASATURATION DENSITIES

NAI-BO ZHANG¹ AND BAO-AN LI^{2*}

¹School of Physics, Southeast University, Nanjing 211189, China

²Department of Physics and Astronomy, Texas A&M University-Commerce, Commerce, TX 75429, USA

*Corresponding author: Bao-An.Li@Tamuc.edu

ABSTRACT

By directly inverting several neutron star observables in the three-dimensional parameter space for the Equation of State of super-dense neutron-rich nuclear matter, we show that the lower radius limit $R_{2.01} \geq 12.2$ km at 68% confidence level for PSR J0740+6620 of mass $2.08 \pm 0.07 M_{\odot}$ from Neutron Star Interior Composition Explorer (NICER)'s very recent observation sets a much tighter lower boundary than previously known for nuclear symmetry energy in the density range of $(1.0 \sim 3.0)$ times the saturation density ρ_0 of nuclear matter. The super-soft symmetry energy leading to the formation of proton polarons in this density region of neutron stars is firmly ruled out by the first radius measurement for the most massive neutron star observed reliably so far.

Keywords: Dense matter, equation of state, stars: neutron

1. INTRODUCTION

The PSR J0740+6620 having an updated mass of $2.08 \pm 0.07 M_{\odot}$ (Fonseca et al. 2021) remains the most massive neutron star (NS) discovered so far (Cromartie et al. 2019). Its radius of $13.7^{+2.6}_{-1.5}$ km (68%) (Miller et al. 2021) or $12.39^{+1.30}_{-0.98}$ km (Riley et al. 2021) was very recently inferred in two independent analyses of the X-ray data taken by the *Neutron Star Interior Composition Explorer* (NICER) and the X-ray Multi-Mirror (XMM-Newton) observatory. Combined with NICER's earlier simultaneous mass and radius measurement of PSR J0030+0451 (Miller et al. 2019; Riley et al. 2019), the first radius measurement of the most massive NS has the strong potential to reveal interesting new physics about the Equation of State (EOS) of super-dense neutron-rich nuclear matter. Besides earlier predictions about what uniquely new physics can be learned from the radii of massive NSs compared to canonical ones, see, e.g., Xie & Li (2020); Han & Prakash (2020); Drischler et al. (2021); Somasundaram & Margueron (2021), several new analyses aiming at extracting new information about the EOS of super-dense matter from NS observations including the latest NICER observations have already been carried out (Biswas 2021; Li et al. 2021; Raaijmakers et al. 2021; Pang et al. 2021). In this Letter, we show that the 68% lower mass-radius boundary of $R_{2.01} \geq 12.2$ km (Miller et al. 2021) provides a much tighter lower boundary than previously known for nuclear symmetry energy in the density range of $(1.0 \sim 3.0)\rho_0$. In particu-

lar, the $R_{2.01} \geq 12.2$ km clearly rules out the super-soft symmetry energy necessary for the formation of proton polarons in this density region in NSs and the associated phenomena predicted in the literature.

The average energy per nucleon $E(\rho, \delta)$ in neutron-rich matter of nucleon density $\rho = \rho_n + \rho_p$ and isospin asymmetry $\delta \equiv (\rho_n - \rho_p)/\rho$ can be written as (Bombaci & Lombardo 1991)

$$E(\rho, \delta) = E_0(\rho) + E_{\text{sym}}(\rho) \cdot \delta^2 + \mathcal{O}(\delta^4) \quad (1)$$

where $E_0(\rho)$ is the nucleon energy in symmetric nuclear matter (SNM) while $E_{\text{sym}}(\rho)$ is the nuclear symmetry energy. The latter measures the energy cost to make nuclear matter more neutron-rich. It is essentially the difference in energy per nucleon in pure neutron matter (PNM) and SNM. The $E_{\text{sym}}(\rho)$ is very poorly known especially at suprasaturation densities mainly because of our poor knowledge about the spin-isospin dependence of three-body nuclear forces, the isospin dependence of the tensor force, and the related short-range nucleon-nucleon correlations in dense neutron-rich matter (Li et al. 2018, 2019). It has been well known that theoretical predictions of high-density $E_{\text{sym}}(\rho)$ diverge broadly at suprasaturation densities, ranging from large negative to positive values at densities above about $(2 \sim 3)\rho_0$ (Li et al. 1998; Steiner et al. 2005; Baran et al. 2005; Li et al. 2008, 2014; Baldo & Burgio 2016). To our best knowledge, there is no fundamental physics principle forbidding the $E_{\text{sym}}(\rho)$ to become zero or even negative at suprasaturation densities. In fact, based

on variational nuclear many-body theory calculations (Pandharipande & Garde 1972; Wiringa et al. 1988), it was pointed out already that when the repulsive short-range tensor force due to the ρ meson exchange in the isosinglet nucleon-nucleon interaction channel in SNM becomes dominating at high densities, the energy in SNM increases faster than that in PNM, leading to a decreasing $E_{\text{sym}}(\rho)$ with increasing density. The $E_{\text{sym}}(\rho)$ may then become zero or even negative above certain critical densities as the $E_{\text{sym}}(\rho)$ is approximately the energy difference between PNM (where the tensor force in the isotriplet nucleon-nucleon interaction channel is known to be negligible) and SNM. Indeed, it was demonstrated quantitatively in Refs. (Xu & Li 2010; Xu et al. 2013) that whether the $E_{\text{sym}}(\rho)$ increases or decreases and when it may become negative depend strongly on properties of the three-body force, the strength and short-range cut-off of the tensor force as well as the related isospin dependence of short-range nucleon-nucleon correlations.

The high-density behavior of $E_{\text{sym}}(\rho)$ has significant ramifications in both nuclear physics and astrophysics (Kutschera & Wójcik 1993; Kutschera 1994; Szmagliński et al. 2006; Baran et al. 2005; Li et al. 2008; Ditoro et al. 2010; Baldo & Burgio 2016; Zhou & Chen 2019). For example, variations of nuclear symmetry energy can lead to large changes in the binding energy and surface curvature of NSs (Newton & Li 2009; He et al. 2015). To further test Einstein’s General Relativity in the strong-field gravity regime against modified gravity theories or the possible existence of a weakly interacting light boson mediating a new force using massive NSs thus requires a reliable knowledge of the high-density $E_{\text{sym}}(\rho)$ (Krivoruchenko et al. 2009; Wen et al. 2009; Lin et al. 2014; Jiang et al. 2015). Moreover, the density profile of proton fraction in NSs at β -equilibrium is uniquely determined by the density dependence of nuclear symmetry energy and has many consequences. For instance, it determines the critical density above which the direct URCA process responsible for the fast cooling of protoneutron stars can happen. In particular, a super-soft $E_{\text{sym}}(\rho)$, i.e., a decreasing/negative symmetry energy at high densities may lead to some very interesting new phenomena in the core of NSs. As the symmetry energy decreases with increasing density, the proton fraction decreases correspondingly, leading to the formation of proton polarons (isolated and localized single or small clusters of protons surrounded by high-density neutrons) (Kutschera & Wójcik 1993; Kutschera 1994) in the core of NSs. It can then strongly affect transport coefficients of NS matter and can produce spontaneous magnetization in NSs (Szmagliński et al. 2006). When the $E_{\text{sym}}(\rho)$ becomes zero at very high densities in

the core of NSs, matter there are completely PNM. Furthermore, if the $E_{\text{sym}}(\rho)$ becomes negative at super-high densities, the so-called isospin separation instability happens (Kutschera 1994; Li 2002), namely, because of the $E_{\text{sym}}(\rho) \cdot \delta^2$ term in the average nucleon energy of Equation (1) in isospin-asymmetric nuclear matter, a uniform symmetric nuclear matter ($\delta = 0$) is unstable energetically against being separated into regions of bulk pure neutron matter ($\delta = +1$) and pure proton matter ($\delta = -1$) when $E_{\text{sym}}(\rho)$ is negative. This may have interesting consequences. For example, it has been shown that a negative $E_{\text{sym}}(\rho)$ has dramatic effects on the possible kaon condensation in the core of NSs (Kubis & Kutschera 2003).

To pin down the high-density behavior of $E_{\text{sym}}(\rho)$ has been a major scientific thrust of high-energy rare isotope beam facilities (U.S. LRP 2015; NuPECC LRP 2017), see, e.g., Tsang et al. (2021); Russotto et al. (2021) for examples of current and planned nuclear reaction experiments probing the high-density $E_{\text{sym}}(\rho)$. In fact, there were some circumstantial evidences for a super-soft $E_{\text{sym}}(\rho)$ at $\rho \geq 1.5\rho_0$ from analyzing data of an earlier heavy-ion reaction experiment (Xiao et al. 2009). However, the conclusion remains controversial (Feng 2012a,b; Xie & Zhang 2014; Jhang et al. 2021) largely due to the strong model dependence and the relatively small isospin asymmetry reached in heavy-ion reactions (Li 2017). Thus, a tight lower boundary for the high-density $E_{\text{sym}}(\rho)$ from measuring the radii of massive NSs are scientifically invaluable for both nuclear physics and astrophysics.

While the radii and tidal deformabilities of canonical NSs provide some useful constraints on the $E_{\text{sym}}(\rho)$ around ρ_0 , they do not constrain significantly the $E_{\text{sym}}(\rho)$ at densities above about $2\rho_0$ as demonstrated clearly already in Zhang & Li (2019a); Xie & Li (2019). This is mainly because the radii and tidal deformabilities of canonical NSs are determined by the nuclear pressure around $(1 \sim 2)\rho_0$ in these relatively light NSs (Lattimer & Prakash 2000, 2004). In fact, it was shown clearly before the GW170817 was discovered that to probe the high-density behavior of $E_{\text{sym}}(\rho)$ one has to use the radii and/or tidal deformabilities of massive NSs while those of the canonical ones only probe the $E_{\text{sym}}(\rho)$ around ρ_0 , see, e.g., Fattoyev et al. (2013, 2014). NICER’s very recent radius measurement of PSR J0740+6620 made this hope a reality for the first time.

The rest of the paper is organized as follows. In the next section, we summarize very briefly the direct inversion approach of analyzing NS observables in the high-density EOS parameter space. We then demonstrate in Section 3 the scientific power of NICER’s radius measurement of PSR J0740+6620 as the most massive NS with a reliable mass in tightening the lower limit of high-

density nuclear symmetry energy. Effects of the remaining uncertainty of the slope parameter L of nuclear symmetry energy will be discussed in Section 4. Finally, we summarize our main findings.

2. DIRECT INVERSION OF NEUTRON STAR OBSERVABLES IN HIGH-DENSITY EOS PARAMETER SPACE

For completeness and ease of our discussions, here we summarize briefly the main features of the NS EOS-metamodel we use in solving the NS inverse-structure problem. More details can be found in our previous publications (Zhang et al. 2018; Zhang & Li 2019a,b,c, 2020; Xie & Li 2019, 2020). We assume the cores of NSs are made of totally charge neutral neutrons, protons, electrons, and muons (the $npe\mu$ model) at β -equilibrium. Unlike the widely used composition-degenerate spectral functions and/or piecewise polytropes that directly parameterize the pressure as a function of energy or baryon density, to probe the high-density symmetry energy we have to keep the isospin dependence of the EOS and retain explicitly the composition information at all densities. For this reason, we metamodel NS EOS by starting at the single nucleon energy level with explicitly isospin dependence. Specifically, we parameterize the $E_0(\rho)$ and $E_{\text{sym}}(\rho)$ according to

$$E_0(\rho) = E_0(\rho_0) + \frac{K_0}{2} \left(\frac{\rho - \rho_0}{3\rho_0} \right)^2 + \frac{J_0}{6} \left(\frac{\rho - \rho_0}{3\rho_0} \right)^3, \quad (2)$$

$$E_{\text{sym}}(\rho) = E_{\text{sym}}(\rho_0) + L \left(\frac{\rho - \rho_0}{3\rho_0} \right) + \frac{K_{\text{sym}}}{2} \left(\frac{\rho - \rho_0}{3\rho_0} \right)^2 + \frac{J_{\text{sym}}}{6} \left(\frac{\rho - \rho_0}{3\rho_0} \right)^3 \quad (3)$$

where $E_0(\rho_0) = -15.9 \pm 0.4$ MeV is the binding energy and $K_0 \approx 240 \pm 20$ MeV (Shlomo et al. 2006; Piekarewicz 2010; Garg & Colò 2018) is the incompressibility at the saturation density ρ_0 of SNM, while $E_{\text{sym}}(\rho_0) = 31.7 \pm 3.2$ MeV is the magnitude and $L \approx 58.7 \pm 28.1$ MeV is the slope of symmetry energy at ρ_0 (Li & Han 2013; Oertel et al. 2017) based on earlier surveys of over 50 analyses of both terrestrial experiments and astrophysical observations, respectively. A very recent survey of 24 new analyses of NS observations since GW179817 indicates that $L \approx 57.7 \pm 19$ MeV and $K_{\text{sym}} \approx -107 \pm 88$ MeV at 68% confidence level (Li et al. 2021). In this study, we use $L = 58.7$ as its most probable value and vary it within ± 20 MeV. We keep the $E_0(\rho_0)$, K_0 , and $E_{\text{sym}}(\rho_0)$ at their most probable values given above as they have been relatively well determined and their variations within their remaining uncertain ranges have been shown to have little effects on the masses, radii, and tidal deformabilities of NSs (Fattoyev et al. 2013, 2014); Xie & Li (2019, 2020).

The K_{sym} , J_{sym} , and J_0 are parameters characteriz-

ing the EOS of super-dense neutron-rich nuclear matter. We directly invert NS observables in the high-density EOS space allowed by the current uncertainties of K_{sym} , J_{sym} , and J_0 as summarized in Zhang et al. (2017). We note qualitatively that while the parameter J_0 (skewness of SNM) controls the stiffness of SNM EOS at high densities, the K_{sym} (curvature of symmetry energy) dominates the behavior of $E_{\text{sym}}(\rho)$ around $2\rho_0$ and the parameter J_{sym} (skewness of symmetry energy) controls the $E_{\text{sym}}(\rho)$ at densities above $(2 \sim 3)\rho_0$. The slope parameter L dominates the behavior of $E_{\text{sym}}(\rho)$ around ρ_0 but does not have much effects on its high-density behavior. It is also known from previous Bayesian analyses and direct inversions that the K_{sym} and J_{sym} affect most strongly on the radii of massive NSs while the L parameter influences most strongly the radii of canonical NSs (Zhang & Li 2019b; Xie & Li 2020).

The pressure in the $npe\mu$ core of NSs is calculated from

$$P(\rho, \delta) = \rho^2 \frac{d\epsilon(\rho, \delta)/\rho}{d\rho}, \quad (4)$$

where $\epsilon(\rho, \delta) = \epsilon_n(\rho, \delta) + \epsilon_l(\rho, \delta)$ denotes the total energy density with contributions from both nucleons ($\epsilon_n(\rho, \delta)$) and leptons ($\epsilon_l(\rho, \delta)$). To see clearly where the symmetry energy comes in, we note in particular that the nucleon energy density $\epsilon(\rho, \delta) = \rho E(\rho, \delta) + \rho M$ with M being the average mass of nucleons. Given the density dependence of nuclear symmetry energy $E_{\text{sym}}(\rho)$, the density profile of isospin asymmetry $\delta(\rho)$ (or the corresponding proton fraction $x_p(\rho)$) is determined by the β -equilibrium and charge neutrality conditions $\mu_n - \mu_p = \mu_e = \mu_\mu$, $\rho_p = \rho_e + \rho_\mu$ in terms of the chemical potential $\mu_i = \frac{\partial \epsilon(\rho, \delta)}{\partial \rho_i}$ and particle density ρ_i of particle i .

We connect the core EOS described above with the NV EOS (Negele & Vautherin 1973) for the inner crust and the BPS EoS (Baym et al. 1971) for the outer crust. The crust-core transition density and pressure are determined consistently for each EOS generated for the core as discussed in detail in Zhang et al. (2018).

Using the metamodel EOS outlined above, for a given observable of NSs one can loop through the 3-dimensional high-density EOS parameter space spanned by the K_{sym} , J_{sym} , and J_0 parameters within their currently known uncertainties. In looping through the entire high-density EOS parameter space, we also require all accepted EOSs to satisfy the causality condition, a specified *minimum* maximum mass of NSs (i.e., the mass of the currently observed most massive NS), dynamical stability through out the entire NS as well as a positive pressure at the crust-core transition density. All accepted EOSs giving the same NS observable will be presented by a constant observable surface in the K_{sym} - J_{sym} - J_0 parameter space. Crosslines of two observable

surfaces and/or those between an observable surface and the causality surface will set boundaries for the acceptable high-density EOS parameter space.

3. THE POWER OF RADIUS MEASUREMENT OF MASSIVE NEUTRON STARS ON CONSTRAINING HIGH-DENSITY NUCLEAR EOS

Shown in Figure 1 are the tightest constraints on the 3D high-density EOS parameter space with $L = 58.7$ MeV from inverting (1) the upper limit of the tidal deformability $\Lambda_{1.4} = 580$ from LIGO/VIRGO (Abbott et al. 2018), (2) the lower radius limit of $R_{2.01} = 12.2$ km for PSR J0740+6620 from Miller et al. (2021). Since the corresponding surface of the upper radius limit $R_{2.15} = 16.3$ km sits on the left of the $\Lambda_{1.4} = 580$ surface, it is not shown here. (3) the lower radius limit of $R_{1.28} = 11.52$ km of PSR J0030+0451 from Riley et al. (2019). While it is on the right of the $R_{2.01} = 12.2$ km surface, it is shown to make a comparison. (4) the causality surface on which the speed of sound equals the speed of light ($v_s^2 = dP/d\rho = c^2$) at the central density of the most massive NS supported by the nuclear pressure at each point with the specific EOS there (Zhang & Li 2019a), and (5) the constant mass of $M=2.01 M_\odot$ which is the lower limit of the newly updated mass of PSR J0740+6620 (Fonseca et al. 2021; Miller et al. 2021; Riley et al. 2021). While it is outside the $R_{2.01} = 12.2$ km surface and thus does not provide a tighter constraint on the EOS, it is shown here to compare the constraint on E_{sym} obtained when only the mass of PSR J0740+6620 is measured with that when both its mass and radius are measured. The black arrows indicate the direction to the allowed EOS space. Since the upper radius limits of both PSR J0740+6620 and PSR J0030+0451 from NICER are on the left of the constant $\Lambda_{1.4} = 580$ surface, they do not provide more stringent constraints on the $E_{\text{sym}}(\rho)$ than the $\Lambda_{1.4} \leq 580$ condition and are thus not shown here. Similarly, the lower radius limit of $R_{2.01} = 11.4$ km for PSR J0740+6620 from Riley et al. (2021) is not shown because it is slightly on the right of that from Miller et al. (2021). It provides a slightly looser constraint on the lower limit of $E_{\text{sym}}(\rho)$ but well within its uncertainty range due to the remaining uncertainty of L as we shall discuss later.

Considering all the NS observations available and the relevant physics conditions, the constrained EOS parameter space is surrounded by the surface of $\Lambda_{1.4} = 580$ from the left, the surface $R_{2.01} = 12.2$ km from the right and below, and the causality condition from the top. In addition, at the left-back corner where the K_{sym} is highly positive (around $0 \sim 100$ MeV) and J_{sym} is around $-200 \sim 200$ MeV, there is a wall (not shown here

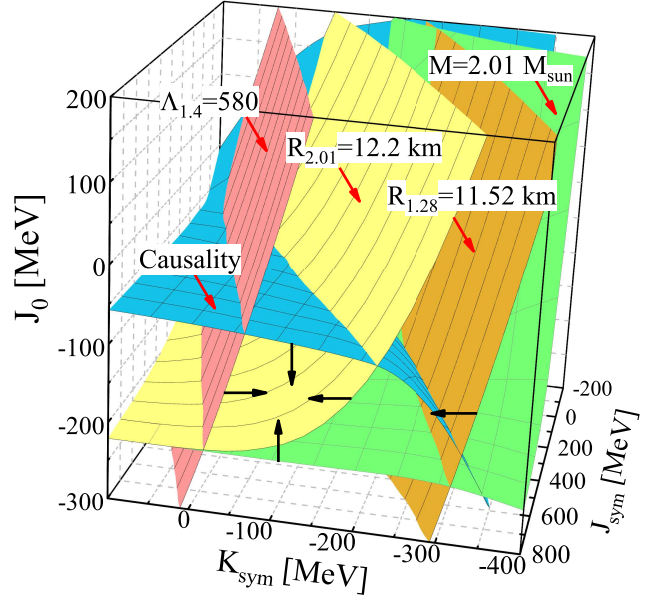


Figure 1. Constant surfaces of NS observables and causality condition in the 3-dimensional $K_{\text{sym}} - J_{\text{sym}} - J_0$ EOS parameter space when L is fixed at its currently known most probable value of $L = 58.7$ MeV: the NS minimum maximum mass of $M = 2.01 M_\odot$ (green surface), the lower limit of radius reported by NICER for PSR J0030+0451 and PSR J0740+6620, i.e., $R_{1.28} = 11.52$ km (orange surface) and $R_{2.01} = 12.2$ km (yellow surface), the dimensionless tidal deformability of canonical NS $\Lambda_{1.4} = 580$ (pink surface), and the causality surface (blue) on which the sound speed equals the speed of light in centers of the most massive NSs. The red arrows point to the corresponding surfaces while the black arrows show directions that satisfy the corresponding constraints.

to avoid crowding) on which the crust-core transition pressure is zero, cutting-off the extremely stiff symmetry energy at very low subsaturation densities (Zhang & Li 2019a).

Several interesting and important observations can be made from comparing the constant surfaces of NS observables and the causality condition as well as their crosslines shown in Figure 1. In particular, we emphasize the following points:

- The $M = 2.01 M_\odot$ (green) surface together with the causality surface (blue) limit the allowed range of the J_0 , thus the high-density SNM EOS. They are essentially vertical to the J_0 axis when the $E_{\text{sym}}(\rho)$ is stiff with large positive K_{sym} and J_{sym} values. This is because when the symmetry energy is stiff, the isospin asymmetry δ at β -equilibrium is small (Quantitatively from solving the equation $\mu_n - \mu_p = \mu_e = \mu_\mu \approx 4\delta E_{\text{sym}}(\rho)$. Qualitatively, it can be understood simply from minimizing the $E_{\text{sym}}(\rho) \cdot \delta^2$ term in Equation (1)). The nuclear pressure is then dominated by the contribution from SNM EOS. However, when the $E_{\text{sym}}(\rho)$ be-

comes super-soft with large negative K_{sym} and/or J_{sym} values, nuclear matter becomes very neutron-rich with large δ values. Then, the symmetry energy contribution to nuclear pressure becomes large and can be even negative. Thus to support the same NS mass $M = 2.01 M_{\odot}$, the SNM EOS has to become stiffer with higher J_0 values, leading to the bending up of the $M = 2.01 M_{\odot}$ surface at the right-back corner where the K_{sym} and/or J_{sym} are largely negative.

On the other hand, for most of the J_{sym} values the causality surface bends downward as the K_{sym} parameter goes from positive to large negative values. As discussed in detail in [Zhang & Li \(2019a\)](#), this is because both the NS maximum mass M_{max} on the causality surface that the EOS can support and the corresponding radius R_{max} decrease when the $E_{\text{sym}}(\rho)$ becomes more soft as the K_{sym} decreases. Since the maximum density ρ_{max} reached in this maximum mass NS scales with $M_{\text{max}}/R_{\text{max}}^3$, it increases very quickly with the decreasing curvature K_{sym} towards super-soft $E_{\text{sym}}(\rho)$. Therefore, the causality condition $v_s = c$ can be reached at much smaller J_0 values as the K_{sym} decreases. We notice that the variation of the causality surface with the skewness parameter J_{sym} is more complicated as its effects on both the maximum mass and the corresponding radius are non-monotonic depending on the SNM EOS parameter J_0 .

Previously, the crossline between the causality surface and the surface representing the NS *minimum* maximum mass observed so far sets the lower boundary for the high-density symmetry energy before the radius of PSR J0740+6620 becomes available. Technically, we notice that since the mass of PSR J0740+6620 has been revised downwards from the preliminary $2.17 M_{\odot}$ to the previously published $2.14 M_{\odot}$ to the current $2.08 M_{\odot}$, its crossline with the causality surface has been varied slightly compared to the earlier one ([Zhang & Li 2019c](#)).

- The power in limiting the EOS parameter space using simultaneously the knowledge about both the mass and radius of a massive NS can be seen clearly from comparing the $M = 2.01 M_{\odot}$ surface and the $R_{2.01} = 12.2$ km surface. There is a huge gap in the direction of J_0 between the two surfaces in the area where the $E_{\text{sym}}(\rho)$ is super-soft. The gap closes gradually as the $E_{\text{sym}}(\rho)$ becomes super-stiff towards the front-left corner. This is understood again because the pressure is dominated by the SNM EOS when the $E_{\text{sym}}(\rho)$ is super-stiff and the corresponding isospin asymmetry δ

vanishes. In this region of the high-density EOS parameter space, the only mechanism to change both the NS mass and its radius simultaneously is through the variation of J_0 .

On the other hand, it is seen that in the space where the $E_{\text{sym}}(\rho)$ is super-soft, the $R_{2.01} = 12.2$ km surface is almost vertical while the $M = 2.01 M_{\odot}$ surface is still rather flat, meaning that the variation of J_0 has essentially no effect on the radius of PSR J0740+6620 in this EOS parameter region. Most importantly, the crossline between the $R_{2.01} = 12.2$ km surface and the causality surface sets the new lower boundary of $E_{\text{sym}}(\rho)$. Compared to the lower boundary set by the crossline between the $M = 2.01 M_{\odot}$ and causality surfaces, it moved upward (become stiffer) significantly as we shall discuss more quantitatively below. While the crossline between the $R_{2.01} = 12.2$ km surface and the $\Lambda_{1.4} = 580$ surface sets the new upper boundary of $E_{\text{sym}}(\rho)$. It is very close to the one set by the crossline between the $\Lambda_{1.4} = 580$ and $M = 2.01 M_{\odot}$ surfaces. Therefore, the most important effect of knowing simultaneously both the radius and mass of the most massive NS observed is in pinning down the high-density symmetry energy especially its lower boundary.

- The power in limiting the EOS parameter space of knowing the radius of a massive NS compared to that of a light one can be clearly seen by comparing the $R_{2.01} = 12.2$ km surface and the $R_{1.28} = 11.52$ km surface. The latter is rather vertical because in the whole EOS space considered, all values of J_0 can support a NS of $M = 1.28 M_{\odot}$ that has a relatively low central density and the J_0 has almost no effect on the radii of light NSs, in contrast to the situation for the most massive NS observed so far as we discussed above. The separation between these two surfaces clearly indicates the strong sensitivity of NS radius to the variation of $E_{\text{sym}}(\rho)$. Since both surfaces are the lower radius limits of the two NSs considered, it is obvious that the $R_{2.01} = 12.2$ km surface provides a more tight lower limit for the $E_{\text{sym}}(\rho)$, while the crossline of the $R_{1.28} = 11.52$ km surface with either the causality or the $M = 2.01 M_{\odot}$ surface gives a lower boundary very close to that from the crossline between the causality and $M = 2.01 M_{\odot}$ surfaces as we discussed above.

As the high-density EOS parameter space has been constrained in Figure 1, we now turn to the corresponding boundaries of the high-density symmetry energy itself. The latter is determined by the K_{sym} and J_{sym}

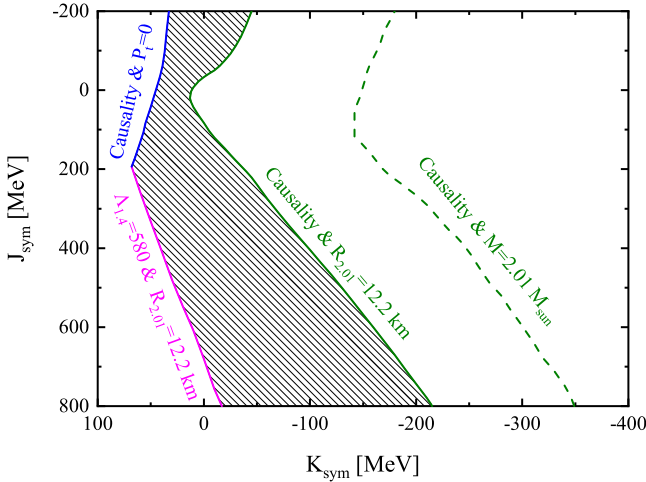


Figure 2. The projection of the constrained space in Figure 1 into the $K_{\text{sym}} - J_{\text{sym}}$ plane for $L = 58.7$ MeV. Each boundary is labeled by the surfaces determining the crosslines. The dash line corresponds to the constraint determined by the crossline between causality and $M = 2.01 M_{\odot}$.

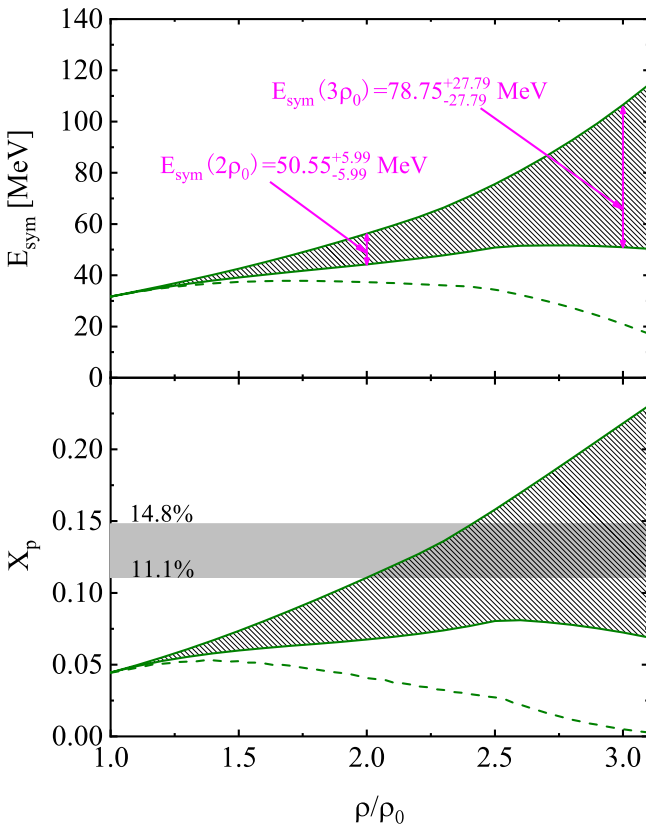


Figure 3. Upper panel: The constrained symmetry energy calculated from the constrained parameter sets in the left panel. Lower panel: The corresponding proton fraction as a function of density. The horizontal shaded range shows the critical proton fraction $11.1\% \sim 14.8\%$ (Klähn et al. 2006) for the direct URCA process to occur. The dash line corresponds to the constraint when only $M = 2.01 M_{\odot}$ is observed.

parameters when the L and $E_{\text{sym}}(\rho_0)$ are fixed at their most probable values given earlier. The allowed band of nuclear symmetry energy can be obtained by projecting the constrained EOS parameter space to the $K_{\text{sym}} - J_{\text{sym}}$ plane as shown by the shadowed area in Figure 2. As indicated in the plot, the boundaries are given by the crosslines we discussed above. In particular, we note that the boundary from the crossline between the causality and $M = 2.01 M_{\odot}$ surfaces sets the lower limit of K_{sym} at -349 MeV. The new information about the radius $R_{2,01} = 12.2$ km for PSR J0740+6620 moves it to about -215 MeV, thus reducing the uncertainty range of K_{sym} by a factor of about 1.6. However, the J_{sym} parameter is still not constrained by the NS observations available. But it can be potentially constrained by future radius measurements of even more massive NSs, messengers directly from the core of NSs, e.g., neutrinos, postmerger high-frequency gravitational waves and/or properties of hyper/super-massive remnants following mergers of two NSs.

Using Equation (3), the boundaries in the K_{sym} versus J_{sym} plane can be translated into constraints for the symmetry energy $E_{\text{sym}}(\rho)$ as shown in the upper panel of Figure 3. Clearly, the measured radius of the most massive NS observed so far improves significantly our knowledge about nuclear symmetry energy especially at densities higher than about $2.5\rho_0$. More specifically, the symmetry energy at $2\rho_0$ and $3\rho_0$ are now constrained to $E_{\text{sym}}(2\rho_0) = 50.55 \pm 5.99$ MeV and $E_{\text{sym}}(3\rho_0) = 78.75 \pm 27.79$ MeV, respectively. These constraints are quantitatively more accurate than our previous results obtained using earlier NS observations (Zhang & Li 2019a). Moreover, a recent survey of 9 independent analyses of NS observations since GW170817 and 2 earlier analyses of heavy-ion reaction experiments gave a fiducial value of $E_{\text{sym}}(2\rho_0) \approx 51 \pm 13$ MeV at 68% confidence level (Li et al. 2021). The $E_{\text{sym}}(2\rho_0) = 50.55 \pm 5.99$ MeV from the present work is consistent with this fiducial value but has an about 50% smaller error bar, indicating a significant refinement due to NICER's radius measurement of PSR J0740+6620.

As mentioned earlier, the density profile of proton fraction $X_P(\rho)$ determined uniquely by the $E_{\text{sym}}(\rho)$ is a critical quantity for addressing several interesting NS physics issues. The constrained proton fraction $X_P(\rho)$ is shown in the lower panel of Figure 3. The direct URCA process is predicted to occur once the proton fraction exceeds the critical fraction of about $11.1\% \sim 14.8\%$ (Klähn et al. 2006). The results indicate that the direct URCA process definitely will not happen below about $2\rho_0$ but remains uncertain at higher densities.

Moreover, the possible formation of proton polarons and several related phenomena as well as the trig-

ger of isospin separation instability in the core of NSs all depend critically on the proton fraction at high densities(Kutschera & Wójcik 1993; Kutschera 1994; Kubis & Kutschera 2003; Szmagliński et al. 2006). One common condition is that the symmetry energy has to start decreasing with increasing density above certain critical density, leading to the gradual disappearance of protons in the core of NSs. From Figure 3, it is seen that the lowest boundary (the dashed line determined by the crossline between the causality and the $M = 2.01 M_{\odot}$ surfaces) of X_p permits this when only the mass $M = 2.01 M_{\odot}$ is observed for PSR J0740+6620. In fact, many phenomenological and microscopic models predicted high-density behaviors of the E_{sym} and the corresponding X_p similar to the dashed line, see, e.g., the 10 realistic EOSs used in Szmagliński et al. (2006) in studying the proton polaron formations in NSs. Interestingly, however, the lower boundary of X_p from using the lower radius limit $R_{2.01} = 12.2$ km rules out firmly the formation of proton polarons at least upto about $3.0\rho_0$. While it still may be possible at higher densities, our present model assuming NSs are made of $npe\mu$ matter may break down and thus can not be used reliably to make predictions at higher densities.

4. EFFECTS OF THE REMAINING UNCERTAINTY OF THE SLOPE PARAMETER L OF NUCLEAR SYMMETRY ENERGY

In the above discussions, the slope L of symmetry energy is set at its fiducial value of $L = 58.7$ MeV, while it is known that it still has an uncertainty of about 20 MeV based on the latest survey of available analyses in the literature (Li et al. 2021). The L parameter characterizes mainly the symmetry energy around ρ_0 . It is well known that L has strong imprints on the radii and tidal deformations of canonical NSs. However, it is unclear how it may affect the radii and masses of massive NSs as well as the causality surface. Most importantly, how does L affect the boundaries of the symmetry energy we extracted above? To address these questions we have re-calculated everything with $L = 40$ and 80 MeV and compared the results with the ones we obtained above with $L = 58.7$ MeV.

Shown in Figure 4 are comparisons of the constant surfaces of $\Lambda_{1.4} = 580$ (upper panel), $R_{1.28} = 11.52$ km (middle panel), and $R_{2.01} = 12.2$ km (lower panel) with $L = 40$, 58.7, and 80 MeV, respectively. As expected, the increase of L shifts the surfaces of $\Lambda_{1.4} = 580$ and $R_{1.28} = 11.52$ km to smaller K_{sym} values. For the light NSs, when L becomes larger, K_{sym} has to become smaller to reproduce the same radii and/or tidal deformabilities. This is consistent with our previous findings shown in Zhang & Li (2019b). Interestingly, however, the above expectation is also true for the radii

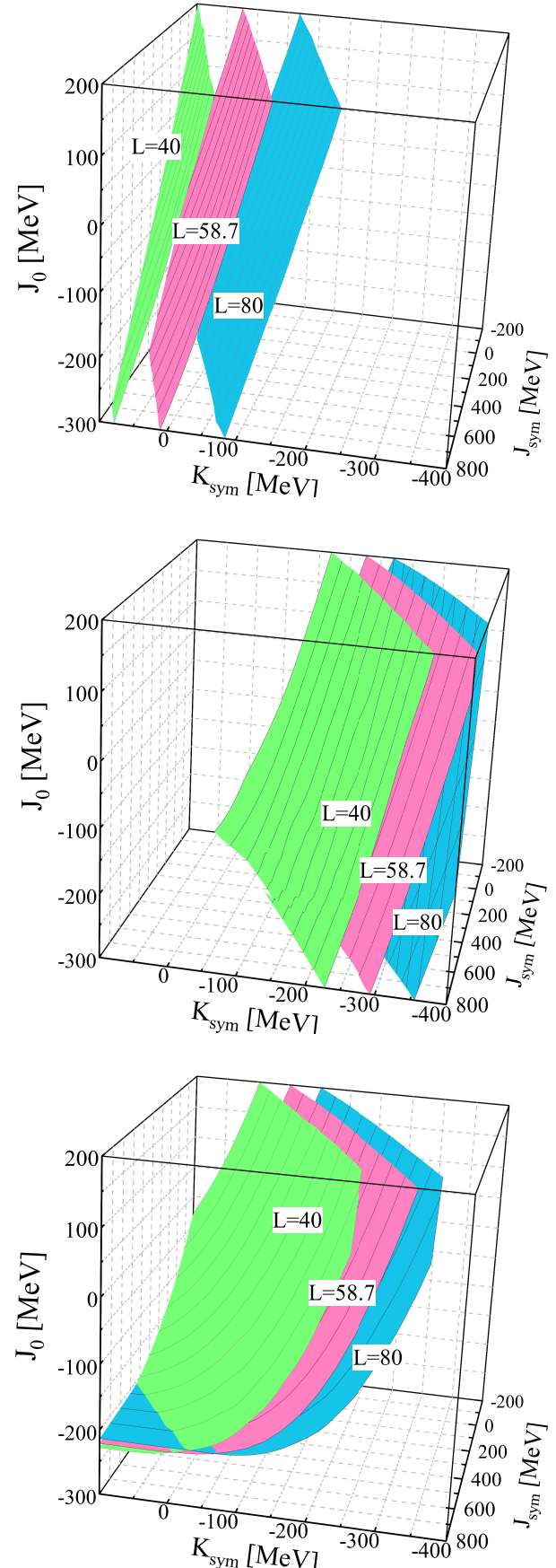


Figure 4. Comparisons of the constant surfaces of $\Lambda_{1.4} = 580$ (upper panel), $R_{1.28} = 11.52$ km (middle panel), and $R_{2.01} = 12.2$ km (lower panel) for $L = 40$, 58.7, and 80 MeV, respectively.

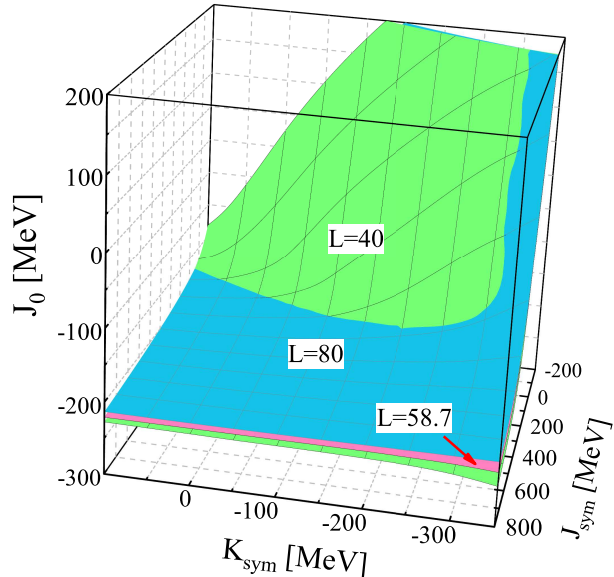


Figure 5. Comparisons of the constant surfaces of mass $M = 2.01 M_{\odot}$ (upper panel) and causality condition (lower panel) for $L = 40, 58.7$, and 80 MeV, respectively.

of massive NSs only in the space where the symmetry energy is super-soft as indicated by the surfaces of $R_{2.01} = 12.2$ km for different L in the lower panel. In the region where the symmetry energy is super-stiff, the L is seen to have little effect on the $R_{2.01} = 12.2$ km surface. As we discussed earlier, when the symmetry energy is stiff (larger K_{sym} and J_{sym}), the pressure is dominated by the SNM EOS, namely the J_0 parameter. Then both the mass and radius are mainly determined

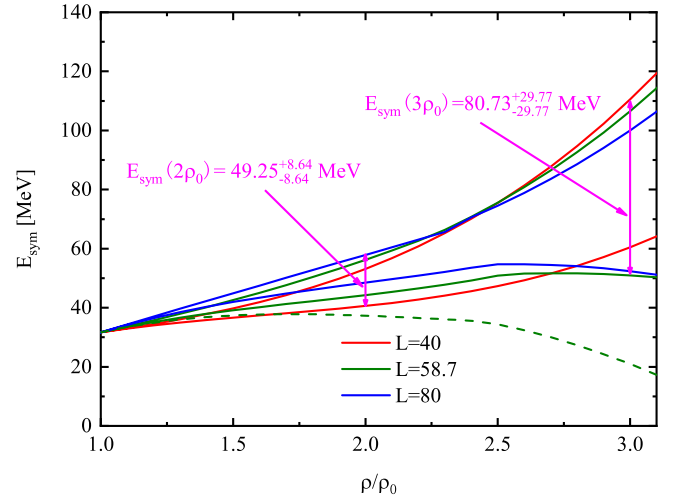


Figure 6. The combined constraints on symmetry energy for $L = 40, 58.7$, and 80 MeV. The dash line corresponds to the constraint of the crossline between the surfaces of causality and $M = 2.01 M_{\odot}$ for $L = 58.7$ MeV.

by the J_0 with little influence from the symmetry energy. Moreover, since the K_{sym} and J_{sym} are both so big in the super-stiff region, the L parameter thus has little effect on the $R_{2.01} = 12.2$ km surface when the symmetry energy is super-stiff. For similar reasons, as shown in Figure 5, the variation of L has little effect on the constant surface of $M = 2.01 M_{\odot}$ and the causality surface, except in the space where the symmetry energy is super-soft.

Since the crosslines determining the boundaries of E_{sym} are not in the super-soft region, effects of L on these boundaries are expected to be small or moderate. Summarized in Figure 6 are constraints on the symmetry energy using $L = 40, 58.7$, and 80 MeV, respectively. Not surprisingly, although the change of L shifts some surfaces appreciably (see Figure 4), the symmetry energy boundaries below $3\rho_0$ are rather robust against the variation of L by ± 20 MeV around its fiducial value. More quantitatively, comparing the values of $E_{\text{sym}}(2\rho_0)$ and $E_{\text{sym}}(3\rho_0)$ shown here and those in Figure 3, it is seen that their mean values remain approximately the same while the error bars only increased slightly.

5. SUMMARY AND CONCLUSIONS

In summary, by directly inverting several NS observables in the high-density EOS parameter space we have shown that the lower radius limit $R_{2.01} \geq 12.2$ km from NICER's very recent observation of PSR J0740+6620 sets a much tighter lower boundary than previously known for nuclear symmetry energy in the density range of $\sim (1.0 - 3.0)\rho_0$. The super-soft symmetry energy leading to the formation of proton polarons and the related phenomena predicted to occur in this density region in the core of NSs is firmly ruled out by NICER's radius

measurement for the most massive NS observed so far.

ACKNOWLEDGEMENT

We would like to thank Wen-Jie Xie for helpful discussions. This work is supported in part by the U.S. Department of Energy, Office of Science, under Award

Number DE-SC0013702, the CUSTIPEN (China-U.S. Theory Institute for Physics with Exotic Nuclei) under the US Department of Energy Grant No. DE-SC0009971, the National Natural Science Foundation of China under Grant No. 12005118, and the Shandong Provincial Natural Science Foundation under Grants No. ZR2020QA085.

REFERENCES

Abbott, B. P., Abbott, R., Abbott, T. D., et al. 2018, *PhRvL*, 121, 161101

Baldo, M., & Burgio, G. F. 2016, *Prog. Part. Nucl. Phys.*, 91, 203

Baran, V., Colonna, M., Greco, V., & Di Toro, M. 2005, *Phys. Rep.*, 410, 335

Baym, G., Pethick, C. J., & Sutherland, P. 1971, *ApJ*, 170, 299

Biswas, B. 2021, arXiv:2105.02886

Bombaci, I., & Lombardo, U. 1991, *PhRvC*, 44, 1892

Cromartie, H. T., Fonseca, E., Ransom, S. M., et al. 2019, *NatAs*, 4, 72

Ditoro, M., Baran, V., Colonna, M., & Greco, V. 2010, *J. Phys. G.*, 37, 083101

Drischler, C., Han, S., Lattimer, J. M., et al. 2021, *PhRvC*, 103, 045808

Fattoyev, F. J., Carvajal, J., Newton, W. G., & Li, B. A. 2013, *PhRvC*, 87, 015806

Fattoyev, F. J., Newton, W. G., & Li, B. A. 2014, *PhRvC*, 90, 022801

Feng, Z. Q. 2012a, *NuPhA*, 878, 3

Feng, Z. Q. 2012b, *Physics Letters B* 707, 83

Fonseca, E., Cromartie, H. T., Pennucci, T. T., et al. 2021, arXiv:2104.00880

Garg, U., & Colò, G. 2018, *Prog. Part. Nucl. Phys.*, 101, 55

Han, S. & Prakash, M. 2020, *ApJ*, 899, 164

He, X. T., Fattoyev, F. J., Li, B. A., & Newton, W. G. 2015, *PhRvC*, 91, 015810

Jhang, G., Estee, J., Barne, J., et al. 2021, *Physics Letters B*, 813, 136016

Jiang, W. Z., Li, B. A., & Fattoyev, F. J. 2015, *EPJA*, 51, 119

Krivoruchenko, M. I., Simkovic F., & Faessler, A. 2009, *PhRvD*, 79, 125023

Klähn, T., Blaschke, D., Typel, S., et al. 2006, *PhRvC*, 74, 035802

Kubis, S., & Kutschera, M. 2003, *Nucl. Phys. A*, 720, 189

Kutschera, M., & Wójcik, W. 1993 *PhRvC*, 47, 1077

Kutschera, M. 1994, *Physics Letters B*, 340, 1

Lattimer, J. M., & Prakash, M. 2000, *Phys. Rep.*, 333, 121

Lattimer, J. M., & Prakash, M. 2004, *Sci*, 304, 536

Li, B. A., Ko, C. M., & Bauer W. 1998, *Int. Jour. Mod. Phys. E*, 7, 147

Li, B. A. 2002, *PhRvL*, 88, 192701

Li, B. A., Chen, L. W., & Ko, C. M. 2008, *Phys. Rep.*, 464, 113

Li, B. A., & Han, X. 2013, *Phys. Lett. B*, 727, 276

Li, B. A., Ramos, Á., Verde G., & Vidaña, I. (Eds.) 2014, *EPJA*, 50, 9

Li, B. A. 2017, *Nuclear Physics News*, 27, 7

Li, B. A., Cai, B. J., Chen, L. W., & Xu J. 2018, *Progress in Particle and Nuclear Physics*, 99, 29

Li, B. A., Krastev, P. G., Wen, D. H., & Zhang, N. B. 2019, *EPJA*, 55, 117

Li, B. A., Cai, B. J., Xie, W. J., & Zhang, N. B. 2021, arXiv:2105.04629

Lin, W., Li, B. A., Chen, L. W., Wen, D. H., & Xu, J. 2014, *JPhG*, 41, 075203

Miller, M. C., Lamb, F. K., Dittmann, A. J., et al. 2019, *ApJL*, 887, L24

Miller, M. C., Lamb, F. K., Dittmann, A. J., et al. 2021, arXiv:2105.06979

Negele, J. W., & Vautherin, D. 1973, *NuPhA*, 207, 298

Newton, W. G., & Li, B. A. 2009, *PhRvC*, 80, 065809

Oertel, M., Hempel, M., Klähn, T., & Typel, S. 2017, *Rev. Mod. Phys.*, 89, 015007

Pandharipande, V. R., & Garde, V. K. 1972, *Physics Letters B*, 39, 608

Pang, P. T. H., Tews, I., Coughlin, M. W., et al. 2021, arXiv:2105.08688

Piekarewicz, J. 2010, *JPhG*, 37, 064038

Raaismakers, G., Greif, S. K., Hebeler, K., et al. 2021, arXiv:2105.06981

Reaching for the Horizon, the 2015 Long Range Plan for Nuclear Science, <https://www.osti.gov/biblio/1296778-reaching-horizon-long-range-plan>

Riley, T. E., Watts, A. L., Bogdanov, S., et al. 2019, *ApJL*, 887, L21

Riley, T. E., Watts, A. L., Ray, P. S., et al. 2021, arXiv:2105.06980

Russotto, P., Le Fèvre, A., Lukasik, J., et al. 2021, arXiv:2105.09233

Shlomo, S., Kolomietz, V. M., & Colò G. 2006, *EPJA*, 30, 23

Somasundaram, R., & Margueron, J. 2021, arXiv:2104.13612

Steiner, A. W., Prakash, M., Lattimer, J. M., & Ellis, P. J. 2005, *Phys. Rep.*, 410, 325

Szmagliński, A., Wójcik, W., & Kutschera, M. 2006, *Acta Phys. Pol. B* 37, 277

The Nuclear Physics European Collaboration Committee (NuPECC), Long Range Plan 2017 Perspectives in Nuclear Physics, https://www.esf.org/fileadmin/user_upload/esf/Nupecc-LRP2017.pdf

Tsang, M. B., et al. 2021, The Symmetry Energy Project, <https://groups.nscl.msu.edu/hira/sepweb/pages/about.html>

Wen, D. H., Li, B. A., & Chen, L. W. 2009, *PhRvL*, 103, 211102

Wiringa, R. B., Fiks, V., & Fabrocini, A. 1988, *PhRvC*, 38, 1010

Worley, A., Krastev, P. G., & Li, B. A. 2008, *ApJ*, 685, 390

Xiao, Z. G., Li, B. A., Chen, L. W., Yong, G. C., & Zhang, M. 2009, *PhRvL*, 102, 062502

Xie, W. J., & Zhang, F. S. 2014, *Physics Letters B*, 735, 250

Xie, W. J., & Li, B. A. 2019, *ApJ*, 883, 174

Xie, W. J., & Li, B. A. 2020, *ApJ*, 899, 4

Xu, C., & Li, B. A. 2010, *PhRvC*, 81, 064612

Xu, C., Li, A., & Li, B. A. 2013, *Journal of Physics: Conference Series*, 420, 012090

Zhang, N. B., Cai, B. J., Li, B. A., Newton, W. G., & Xu, J. 2017, *Nucl. Sci. Tech.*, 28, 181

Zhang, N. B., Li, B. A., & Xu, J. 2018, *ApJ*, 859, 90

Zhang, N. B., & Li, B. A. 2019, *EPJA*, 55, 39

Zhang, N. B., & Li, B. A. 2019, *JPhG*, 46, 014002

Zhang, N. B., & Li, B. A. 2019, *ApJ*, 879, 99

Zhang, N. B., & Li, B. A. 2020, *ApJ*, 883, 61

Zhou, Y., & Chen, L. W., 2019, *ApJ*, 886, 52